Contents list available at CBIORE journal website

International Journal of Renewable Energy Development

Journal homepage: https://ijred.cbiore.id

Research Article

Analysis of a standing wave thermoacoustic engine with multiple unit stages

Prastowo Murti[a*], Ikhsan Setiawan[b], Jihan Zeinyuta Rosafira[a], Adhika Widyaparaga[a], Wijayanti Dwi Astuti[c], Tetsushi Biwa[d]

[a]*Department of Mechanical and Industrial Engineering, Faculty of Engineering, Universitas Gadjah Mada, Jl. Grafika No. 2, Yogyakarta 55281, Indonesia*

[b]*Department of Physics, Faculty of Mathematics and Natural Sciences, Universitas Gadjah Mada, Jl. Grafika No. 2, Yogyakarta 55281, Indonesia*

[c]*Department of Electrical Engineering and Informatics, Vocational collage, Universitas Gadjah Mada, Yogyakarta 55281, Indonesia.*

[d]*Department of Mechanical Systems Engineering, Tohoku University, 6-6, Aramaki, Aoba-ku, Sendai 980-8579, Japan.*

Abstract. The thermoacoustic engine is an eco-friendly technology capable of harnessing solar and waste energy for electricity generation, in conjunction with a linear alternator, and can function as a heat pump. This engine type holds significant appeal due to its simplistic design, devoid of any mechanical moving components, comprising only a stack sandwiched between heat exchangers within a resonator. When the temperature gradient across the stack reaches the critical threshold (onset temperature), the working gas undergoes spontaneous oscillation. Typically, a high onset temperature is necessary to induce gas oscillation in a thermoacoustic engine due to viscous losses within the system. A method to lower the onset temperature by increasing the number of unit stages consisting of stacks and heat exchangers so that the engine can utilize low-grade thermal sources has been developed to overcome this challenge. However, this method has only been applied to traveling-wave thermoacoustic engines. Its application in standing-wave engines, which offer a more compact and straightforward structure, remains unexplored. This research aims to examine how the number of unit stages in a standing-wave thermoacoustic engine influences the onset temperature and acoustic field. The onset temperature is estimated using a fundamental hydrodynamics equation and the investigation of the acoustic field throughout the engine using DeltaEC software. Results showed that the strategic positioning of multiple unit stages is essential to achieve a low onset temperature. The minimum onset temperature, approximately 92°C, is obtained when three- or four-unit stages are installed. Additionally, increasing the number of unit stages does not affect the acoustic impedance and phase difference between pressure and velocity in the stack, while simultaneously enhancing both acoustic power output and thermal efficiency.

Keywords: thermoacoustic, standing wave, multiple unit stage, acoustic field, onset temperature.

Received: 13th Feb 2024; Revised: 28th April 2024; Accepted: 15th May 2024; Available online: 27th May 2024

1. Introduction

Owing to the constrained access to fossil fuels and the escalating environmental concerns regarding pollution, eco-friendly technologies dependent on renewable energy reservoirs are consistently being advocated (Rahman, Rahman, and Akter, 2023). With this initiative in mind, efforts have concentrated on the design of a thermoacoustic engine that seamlessly converts thermal energy into acoustic energy, which can be used to produce electricity through electrodynamic transducer (Jaworski and Mao, 2013; Hamood *et al.*, 2018; Timmer, de Blok and van der Meer, 2018). Alternatively, when employed in thermoacoustic refrigerators, it can induce a heat-pumping effect (Yazaki, Biwa and Tominaga, 2002; Ueda *et al.*, 2004; Tijani and Spoelstra, 2008; Murti, Shoji and Biwa, 2023). With its straightforward design and minimal components (such as a stack/regenerator, heat exchanger, and resonator), this engine can help reduce maintenance costs. It also boasts high reliability and environmental friendliness, with its working gas classified as a non-greenhouse gas (Li *et al.*, 2014; Setiawan *et al.*, 2019; Chi *et al.*, 2021).

According to the phase difference between the pressure and velocity waves in the stack/regenerator, thermoacoustic engines can be divided into two main categories: standing- and traveling-wave engines. In pure standing-wave devices, a 90° phase lag occurs between the pressure and velocity waves. In pure traveling-wave devices, the pressure and velocity waves are essentially in phase. These phase differences regulate the timing of the contraction and expansion of a gas parcel within the working fluid in relation to its movement through a porous solid material. This material is referred to as a stack in standing-wave engines or a regenerator in traveling-wave engines (Swift, 2017). In efficiency terms, traveling-wave engines typically exhibit higher thermal efficiency compared to standing-wave engines. It was because of specific acoustic impedance in the traveling wave engine was higher than standing wave one. The high specific acoustic impedance Z led to a reduction in viscous

* Corresponding author
Email: prastowomurti@ugm.ac.id (P. Murti)

https://doi.org/10.61435/ijred.2024.60098
ISSN: 2252-4940/© 2024.The Author(s). Published by CBIORE

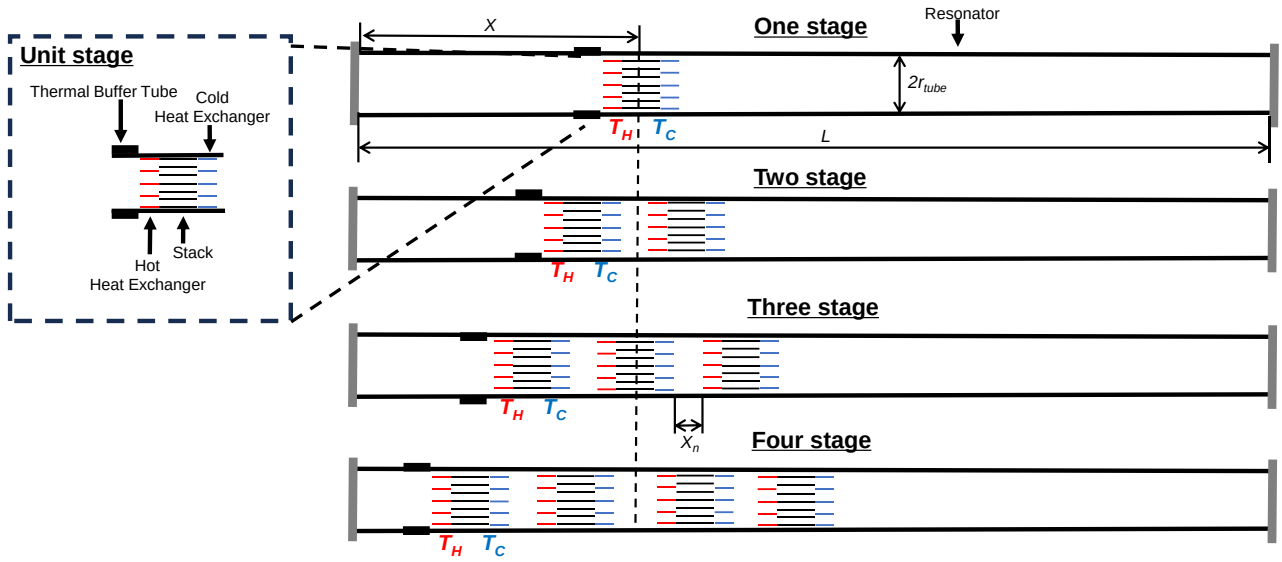

Fig. 1 Schematic diagram of standing wave thermoacoustic engine with multiple unit stages.

losses induced by the gas oscillations in the narrow channel, which given as (Backhaus and Swift, 1999)

$$Z = \frac{p_1}{u_1} \tag{1}$$

where p_1 and u_1 denote complex amplitude of pressure and velocity of the gas, respectively (Hyodo, Tamura and Biwa, 2017). In addition to the higher efficiency seen in traveling-wave thermoacoustic devices, standing-wave types offer advantages stemming from their straightforward configuration, resulting in comparatively lower manufacturing costs. This feature is attributed to the simplicity of accommodating standing-wave phasing using a basic straight resonator (Murti *et al.*, 2016; Piccolo, 2018). On the other hand, traveling-wave types are associated with an intricate and challenging construction that usually requires a loop tube and a resonator (Backhaus and Swift, 2000).

When the heat exchangers impose the temperature gradient on the stack/regenerator, gas oscillation is induced by the oscillation frequency of the resonator's natural frequency. The minimum temperature between the ends of stack to induce oscillation is called onset temperature. Thermoacoustic engines are used to harness low-grade heat sources because the onset temperature can be below 100°C. This accomplishment is attributed to (de Blok Kees, 2012), who suggested a multistage thermoacoustic engine, installed four-unit regenerators on a mutual distance of 1/4 wavelength in each side of the loop, and enlarged the regenerator's cross-sectional area with respect to the looped tube diameter (de Blok, 2010). This setup ensured traveling wave phasing occurred in the regenerator and elevated specific acoustic impedance while reducing the onset temperature difference to as low as 70°C. Thereafter, the multi-stage thermoacoustic systems were reported by many researchers (Li *et al.*, 2013a; Wu *et al.*, 2014; Wang *et al.*, 2016; Zhang *et al.*, 2016; Jin, Yang and Wang, 2017; Tamura, Hyodo and Biwa, 2018). However, it is important to note that these multi-stage thermoacoustic engines have only been applied to the traveling wave configuration, and their suitability for the standing-wave configuration is yet to be addressed.

Therefore, this study aims to numerically analyze the influence of the number of unit stages on the performance of standing-wave thermoacoustic engines. Its effect on the onset temperature will be examined through the stability analysis of thermoacoustic gas oscillations, whereas the acoustic field distribution along the engine was investigated using DeltaEC, a computer program developed by the Los Alamos laboratory based on the thermoacoustic theory. Based on the test results obtained by several researchers (Clark, Ward and Swift, 2007; Yu, Jaworski and Backhaus, 2012; Li *et al.*, 2013; Swift, 2017; Ramadan *et al.*, 2021; Murti, Shoji and Biwa, 2023), this program is accepted as a helpful tool to predict the performance of a thermoacoustic engine.

2. Thermoacoustic engine model

2.1 Model description

Figure 1 presents the model of a standing wave thermoacoustic engine for numerical calculations. It comprises a closed ends resonator with total length L and diameter of $2r_{tube}$, a thermal buffer tube, and a unit stage. The unit stage consists of a hot heat exchanger, a stack, and a cold heat exchanger. The first unit stage is placed at distance X from the middle of average position of unit stages to the closed end, whereas the additional unit stages are arranged in series with a distance between each unit stage of X_n. The stack consists of a porous material had a bundle of cylindrical tubes, each with a radius of r_0 and a length of L_{stk}. The heat exchangers are the parallel-plate type, with a distance r_d between the plates and a length of L_{HX}. Thermal buffer tube is an empty tube with diameter of $2r_{tube}$ and a length of L_{tbt}, and is assumed to have a temperature gradient.

2.2 Stability limit analysis

Stability analysis of thermoacoustic gas oscillations was performed using the transfer matrix method, which is based on the simultaneous linear differential equations proposed by Rott (Rott, 1969, 1975). A presupposition of these equations is that acoustic fluctuations exhibit a temporal dependence in the form

of $e^{i\omega t}$, and are incorporated into the linearized fundamental equations of hydrodynamics to derive a characteristic equation for a particular thermoacoustic system. This characteristic equation is defined by boundary conditions and the type of working fluid. The solution can be expressed utilizing the complex angular frequency $\omega = \omega_R + i\omega_I$. In addition, long wavelength approximations were employed to simplify the equations. As a consequence, the momentum and continuity equations can be expressed as a pair of ordinary differential equations (Swift, 1988; Tominaga, 1995) for the complex amplitude p_1 of pressure and v_1 of volume velocity (Hiroaki, Keita and Tetsushi, 2017)

$$\frac{dp_1}{dx} = -Rv_1 \tag{2}$$

$$\frac{dv_1}{dx} = -Yp_1 + Gv_1. \tag{3}$$

In Eqs. (2) and (3), R, Y, and G are given by

$$R = -i\omega\frac{\rho_m}{A}\frac{1}{1-\chi_v} \tag{4}$$

$$Y = i\omega\frac{A[1+(\gamma-1)\chi_\alpha]}{\gamma P_m} \tag{5}$$

$$G = \frac{\chi_\alpha-\chi_v}{(1-\chi_v)(1-Pr)}\frac{1}{T_m}\frac{dT_m}{dx}, \tag{6}$$

where T_m, ρ_m, and P_m are the temporal averages of gas temperature, density, and pressure of working gas, respectively; γ and Pr denote the specific heat ratio and the Prandtl number, respectively; and A is a cross-sectional area of channel. The thermoacoustic function χ_j ($j = \alpha, v$) was established using the first-order and zeroth-order Bessel functions J_1 and J_0 of the first kind as

$$\chi_j = \frac{2J_1\left[(i-1)\sqrt{\omega\tau_j}\right]}{(i-1)\sqrt{\omega\tau_j}J_0\left[(i-1)\sqrt{\omega\tau_j}\right]} \tag{7}$$

for a circular cylinder, and it is given as

$$\chi_j = \frac{tanh\left[(i-1)\sqrt{\omega\tau_j}\right]}{(i-1)\sqrt{\omega\tau_j}} \tag{8}$$

for a paralel plate. In both equations, τ_j is written as

$$\tau_j = \frac{r^2}{2j} \tag{9}$$

where r is the radius of a circular cylinder. The coupled equations (2) and (3) were solved analytically by treating R, Y and G as constants. The results are expressed as

$$\begin{bmatrix}p_1(x+l)\\v_1(x+l)\end{bmatrix} = M\begin{bmatrix}p_1(x)\\v_1(x)\end{bmatrix} \tag{10}$$

where the transfer matrix M is expressed by (Hiroaki, Keita and Tetsushi, 2017)

$$M = e^{\frac{Gl}{2}}\begin{bmatrix}-\frac{G}{b}sinh\lambda + cosh\lambda & \frac{2R}{b}sinh\lambda\\ \frac{2Y}{b}sinh\lambda & \frac{G}{b}sinh\lambda + cosh\lambda\end{bmatrix} \tag{11}$$

with $b = \sqrt{G^2+4YZ}$ and $\lambda = bl/2$, where l is length of channel segment.

The transfer matrix for the stack M_S with $r = r_0$ and $l = L_{stk}$ is expressed using Eq. (11). To model the stack, we divided it into 10 segments and assumed that the temperature distribution is linear within each segment. Similar to that for the stack matrix, the transfer matrix for the thermal buffer tube M_B can be obtained using the pore radius of resonator r_{tube} and $l = L_{tbt}$ in Eq. (11) and then taking the product of 10 segments. Given that the thermal buffer tube and unit stage occupy the resonator, the rest of the tube has a transfer matrix M_T, which is also given by Eq. (11). Owing to the lack of temperature difference, we used the relation $G = 0$ for this case. In this study, the heat exchangers have a parallel-plate configuration, and their transfer matrix M_{HX} takes the following form:

$$M_{HX} = e^{\frac{Gl}{2}}\begin{bmatrix}cosh\lambda' & \sqrt{\frac{Y}{R}}sinh\lambda\\ \sqrt{\frac{Y}{R}}sinh\lambda' & cosh\lambda'\end{bmatrix} \tag{12}$$

where $\lambda' = L_{HX}\sqrt{YZ}$. The thermoacoustic function χ_j' ($j = \alpha, v$) is replaced with (Swift, 1988; Tominaga, 1995)

$$\chi_j = \frac{tanh\left[(i-1)\frac{r_d}{\delta_j}\right]}{(i-1)\frac{r_d}{\delta_j}}, \tag{13}$$

where r_d is plate distance. Assuming uniform temperatures in the hot T_H and cold T_C heat exchanger regions, we accounted for the temperature-dependent nature of v and α by employing matrix components that vary in these regions. To elucidate these dependencies, we use M_{HH} and M_{CH} to respectively represent the transfer matrix for the hot and cold heat exchangers, respectively. As shown in Fig. 1, the engine with a single-stage unit is composed of a thermal buffer tube, cold heat exchanger, stack, hot heat exchanger, and tube, respectively, as x goes from 0 to L. Thus, the transfer matrix corresponding to the whole straight tube thermoacoustic engine is expressed as

$$M_{all} = M_B M_{HH} M_S M_{CH} M_T. \tag{14}$$

The transfer matrix M_{all} for two-stage, three-stage, and four-stage and so on was expressed by adding the number of transfer matrix M_B, M_{CH}, M_{HH}, and M_S while reducing the tube length l in M_T to keep L constant. When the complex amplitude of pressure and volume velocity at $L = 0$ are p_0 and v_0, whereas the pressure and volume velocity at L are expressed as p_L and v_L, then the Eq. (9) can be rewritten as

$$\begin{bmatrix}p_L\\v_L\end{bmatrix} = M_{all}\begin{bmatrix}p_0\\v_0\end{bmatrix} \tag{15}$$

Given that the resonator has closed ends, the volume velocity at $L = 0$ and L must be zero. Therefore, Eq. (15) can be modified as

$$\begin{bmatrix}p_L\\0\end{bmatrix} = M_{all}\begin{bmatrix}p_0\\0\end{bmatrix}. \tag{16}$$

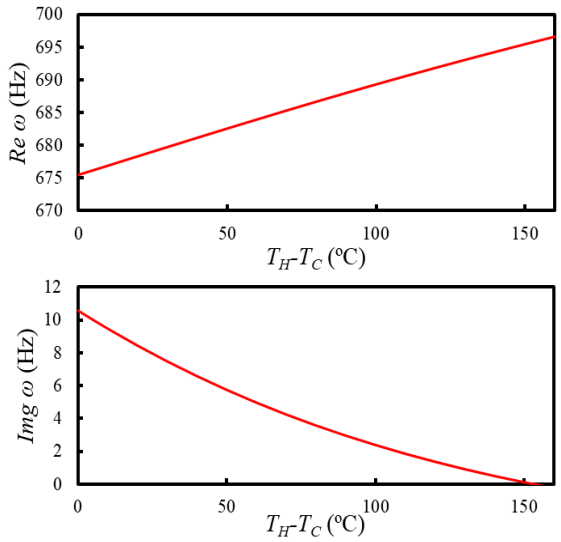

Fig. 2 Influence of temperature difference (T_H-T_C) on real part ω_R (a) dan imaginary part ω_I (b) of the standing-wave thermoacoustic engine.

Eq. (16) have a non-trivial solution if

$$m_{21} = 0, \tag{17}$$

where m_{21} is the element of M_{all}.

To numerically determine the solution for Eq. (17), the angular frequency ω is considered by giving a value of hot heat exchanger temperature T_H and the number of stage units. We applied Newton's method using either ω_0 or ω_1 as the initial values, both of which have a nonzero imaginary component (Hiroaki, Keita and Tetsushi, 2017). The solution of ω is generally a complex quantity of which the real part ω_R represents the angular frequency of fluctuation, while the imaginary part ω_I reflects the system stability. A positive imaginary part indicates that the system is linearly stable, and a negative one indicates that the system is unstable. Therefore, we must find the values of T_H and T_C that lead to a negative ω_I, which indicates that self-sustained gas oscillation has occurred (Hiroaki, Keita and Tetsushi, 2017).

The influence of temperature difference between ends of stack on the real part ω_R and the imaginary part ω_I of the complex frequency of proposed model, shown in Fig. 2(a) and 2(b). It can be observed in Fig. 2(a) that ω_R increases monotonically with T_H-T_C. Conversely, in Fig. 2(b), ω_I gradually moves from positive to negative values, crossing $\omega_I = 0$ when T_H-T_C = 150°C. $\omega_I = 0$ represents the moment just before spontaneous oscillations occur, also known as the critical temperature. Therefore, the onset temperature is determined in the calculations when $\omega_I < 0$ (negative) (Hiroaki, Keita and Tetsushi, 2017).

2.3 DeltaEC program

The DeltaEC program was used to determine the influence of the number of stages on the acoustic field distribution along a standing-wave thermoacoustic engine. DeltaEC uses a 1D approximation of the geometry of the thermoacoustic system and the energy flow (Clark, Ward and Swift, 2007). In DeltaEC, the system is simulated as a sequence of segments which defined by the user such as ducts, heat exchangers, regenerator, and more. The program ensures matching pressure and volumetric velocity, both real and imaginary, at the boundaries of adjacent segments. Acoustic variables at each segment are

Fig. 3 Block diagram of the segments in the standing wave thermoacoustic engine.

determined using the shooting method to satisfy the boundary conditions (targets), which are either set or fixed, such as the volume velocity at the rigid end and the temperature of the ambient heat exchanger. The guesses, for example, initial pressure, volume velocity, temperature, and heat input to the heat exchanger, must be adjusted to meet the targets. If the targets do not match (divergence), then the guess is adjusted and the integration is repeated until convergence is achieved.

The DeltaEC model of a standing wave thermoacoustic engine comprises segments of the thermal buffer tube, hot heat exchanger, stack, cold heat exchanger, and tube, shown in Fig. 3. With the transfer matrix M_{all}, the DeltaEC model of a multistage engine was constructed by including additional segments of the thermal buffer tube, hot and cold heat exchanger, and stack after the first unit stage. The geometries of the segments in the DeltaEC model are set based on the thermoacoustic engine model in subsection 2.1. The working fluid is air at atmospheric pressure and temperature. The boundary conditions are the volume velocity amplitude of tube ends are zero and the temperature conditions for the solid temperatures of the cold and hot heat exchangers, which are 23°C and 180°C, respectively.

3. Experimental verification

3.2 Experiments setup

To verify the model, we built one stage standing wave thermoacoustic engine with specifications as follows: the resonator tube had an internal radius r_{tube} = 0.2 m and a length of L = 1.61 m. The thermal buffer tube length L_{tbt} was 0.165 m. The stack was made of a cylindrical ceramic honeycomb catalyst support, which had square pores with a side of 0.395 mm and a L_{stk} = 35 mm length Both the hot and cold heat exchangers were made of parallel plates having L_{HX} = 10 mm long, 0.5 mm thick parallel plates with a spacing of r_{HX} = 1 mm. Air at atmospheric pressure and temperature was used as a working gas. The temperature of hot heat exchanger T_H was increased using an electrical heater, while the cold heat exchanger temperature T_C was maintained at 23°C using circulating water. Pressure oscillations were monitored using pressure transducers that was placed along the resonator. K-type thermocouples were placed in hot and cold heat exchangers to monitor the temperature of T_H and T_C. Pressure transducer and thermocouples are connected to a personal computer.

3.2 Experiments and calculations comparison

The onset temperature condition of the standing-wave thermoacoustic engine was evaluated with respect to the quality factor (Q-value). The Q-value serves as a measure of the damping level within a thermoacoustic engine and reflects the degree of dissipation. It can be used to assess the extent of damping in the thermoacoustic engine. A high Q-value indicates minimal dissipation, facilitating the generation of self-sustained gas oscillations (Biwa *et al.*, 2005). The Q-value was calculated using $Q = 2\omega_I/\omega_R$, where ω_R and ω_I were obtained from the solution of ω in subsection 2.2.

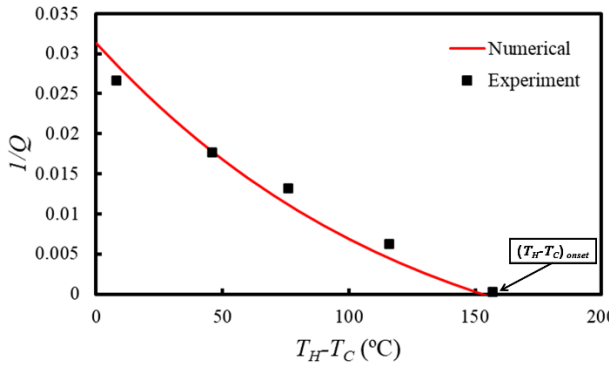

Fig. 4 1/ Q as a function of T_H-T_C. The black square denotes the experimental result.

Figure 4 shows the inverse of quality factor 1/Q as a function of temperature difference between ends of stack T_H-T_C. The red line and black square denote the calculation and experimental results, respectively. As the T_H-T_C increases, the calculated 1/Q for the engine decreases. This reduction in 1/Q signifies an increase in the generation of acoustic power relative to energy dissipation. The onset temperature difference $(T_H\text{-}T_C)_{onset}$ of the engine is determined when 1/Q reaches zero. At this point, the acoustic power production in the regenerator becomes sufficiently high to counterbalance the energy dissipation, thus allowing for the induction of gas oscillation. The calculation result was confirmed by experiment, as shown in Fig. 4. The quality factor is determined by providing acoustic excitation by striking the closed end of the resonator using palm of hand. The resonance curve of damping pressure from external acoustic oscillation was monitored using a pressure transducer and recorded using an FFT analyzer. The Q-value was assessed as $Q = f/\Delta f$, where f represents the peak frequency, and Δf denotes the peak width at half the maximum, which can be determined by fitting the resonance curve to a Lorentz curve. The finding showed that the experimental and numerical results of 1/Q show a good agreement.

Figure 5 shows DeltaEC result for the pressure amplitude P_a, velocity amplitude V, and acoustic power W distribution along the resonator. The shaded area indicates the stack's location. The figure shows 1/2 wavelength generated along the resonator with pressure antinodes at both the ends while the velocity antinode is at the center, indicating thermoacoustic engine as standing wave type. In addition, the stack generates acoustic power W, which is then divided into two directions. In the -x direction, W dissipates through the hot heat exchanger and thermal buffer tube. Meanwhile, in the +x direction, W is dissipated by the cold heat exchanger and resonator. For the verification the DeltaEC result, pressure transducer was used to record the pressure amplitude P_a, then the acoustic power was measured using two sensor method (Biwa *et al.*, 2008). The finding showed that the measured pressure amplitude and acoustic power exhibit good agreement with the DeltaEC. Thus, the stability analysis and DeltaEC accurately reflect the actual condition of the engine and can be employed to determine how its multiple unit stages influences its onset temperature and the acoustic field.

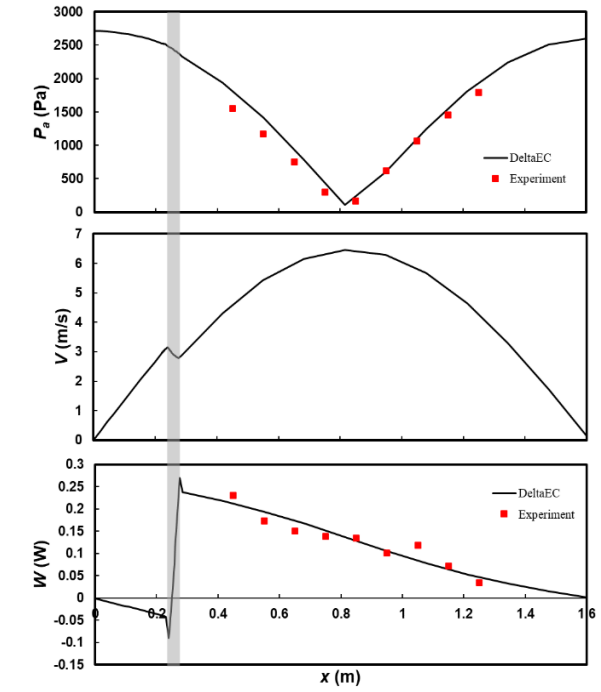

Fig. 5 Distribution of pressure amplitude P_a, velocity amplitude V, and acoustic power W along the standing wave thermoacoustic engine.

4. Result and discussion

The stack should be placed close to the pressure antinode to reduce the viscous dissipation caused by gas oscillation in a narrow channel. However, to produce high acoustic power, it is necessary to position the stack at a pressure node Therefore, the stack must be installed in an optimum position (Swift, 2017). Figure 6 depicts the onset temperature difference $(T_H-T_C)_{onset}$ as a function of the distance of the middle position of unit stage to the closed end of the resonator X, as shown in Fig. 1. For one unit stage, the calculation results indicated that gas oscillations did not occur when X was below 0.11 m but commenced at X = 0.12 m, with $(T_H-T_C)_{onset}$ = 308 °C. Further increases in X resulted in a reduction in $(T_H-T_C)_{onset}$, which then started to increase again after X = 0.26 m. Therefore, the optimal position for the one unit stage is X = 0.26 m because it can attain the lowest $(T_H-T_C)_{onset}$ = 137°C. A similar approach to that of a single unit stage is used for two to six unit stages to understand the position dependence of the multiple unit stages on the onset temperature difference. In this study, the distance between unit stages was set to 40 mm. In Fig. 6, we observed that for all unit stages, the onset temperature decreases with increasing X, but

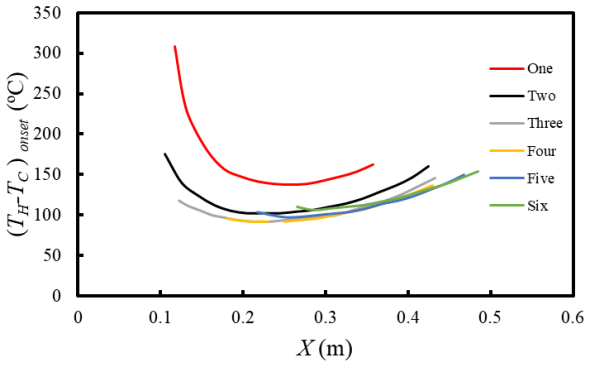

Fig. 6 Onset temperature difference $(T_H\text{-}T_C)_{onset}$ as a function of unit stages position X.

after X = 0.26 m, the onset temperature begins to increase following a pattern similar to that of one unit stage. According to Fig. 5, X = 0.26 m is close to the pressure node and the velocity antinode, where viscous dissipation is low; thus, a low onset temperature difference can be achieved.

Figure 7 shows the onset temperature difference $(T_H-T_C)_{onset}$ as a function of the number of unit stages at X = 0.26 m. We observed that the T_H-T_C of a single unit stage was 137°C. After a second unit stage was installed, the $(T_H-T_C)_{onset}$ decreased to 104°C. With further increase in the number of stages, the onset temperature reached 92°C for the four stages. Meanwhile, the $(T_H-T_C)_{onset}$ of the five-stage configuration increased to 98°C, and this trend continued with the further incorporation of additional stages. This result indicated that the energy dissipation decreases as the number of unit stages increases, leading to a reduction in the onset temperature difference (Biwa, Hasegawa and Yazaki, 2010). Nevertheless, the onset temperature ratio tends to rise when the number of unit stages are further increased, leading to an increase in the energy dissipation of the engine. Therefore, there is optimum number of unit stages for standing wave thermoacoustic engine.

Figure 8 shows the DeltaEC simulation results of acoustic fields in the multi-stage standing wave thermoacoustic engine. We only performed simulations for one to four-unit stages because they achieved the lowest onset temperature. Figure 8(a) shows that the pressure is maximum at the closed ends and minimum close to the middle of the resonator for all unit stages. Conversely, Fig. 8(b) shows that the velocity was the maximum in the middle and minimum at the closed ends. Moreover, increasing the number of unit stages increased the magnitude of the pressure and velocity of the engine. Specifically, four stages drastically increased the pressure and velocity amplitudes, achieving maximum values of 36 kPa and 43 m/s, respectively.

Table 1
Summary of total acoustic power generation and thermal efficiency

Unit stage	Total acoustic power production (W)	Thermal efficiency (%)
Single	0.28	1.4
Two	3.8	1.41
Three	10.03	1.66
Four	22.35	2.57

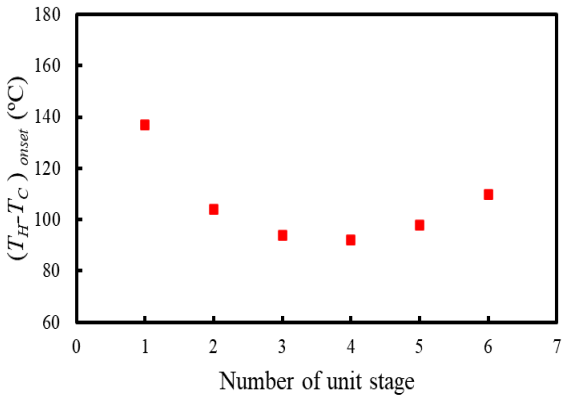

Fig. 7 Onset temperature difference $(T_H-T_C)_{onset}$ in relation to the number of unit stages at X = 0.26 m.

Figure 8(c) shows the phase difference between pressure and velocity Θ_{P-V} along the engine. The Θ_{P-V} in the stack regions for all unit stages was 90°, indicating that standing-wave phasing was achieved. As shown in Fig. 8(d), the minimum and maximum specific acoustic impedance $Z/\rho c$ were found in the middle and closed ends of the resonator, respectively. When the number of unit stages was increased, no significant change in the specific acoustic impedance was observed within the stack region, remaining around $Z/\rho c$ = 2–3. This value is considerably smaller than that of a traveling-wave thermoacoustic engine, which can achieve $Z/\rho c$ = 30 (Backhaus and Swift, 1999). A high $Z/\rho c$ reduces viscous losses due to the gas oscillation in the narrow channel and increases the thermal efficiency.

Figure 8(e) shows the acoustic power W distribution along the resonator. The acoustic power W was produced within the all-stack region and dissipated at the resonator, heat exchangers, and thermal buffer tube regions. Figure 8(e) shows that in the two-unit stage, the first stack generated 0.99 W acoustic power, and the second stack produced a larger amount of W at approximately 2.8 W. This pattern was also observed in the three- and four-unit stages, wherein the initial stage generated a small amount of W, followed by a gradual increase

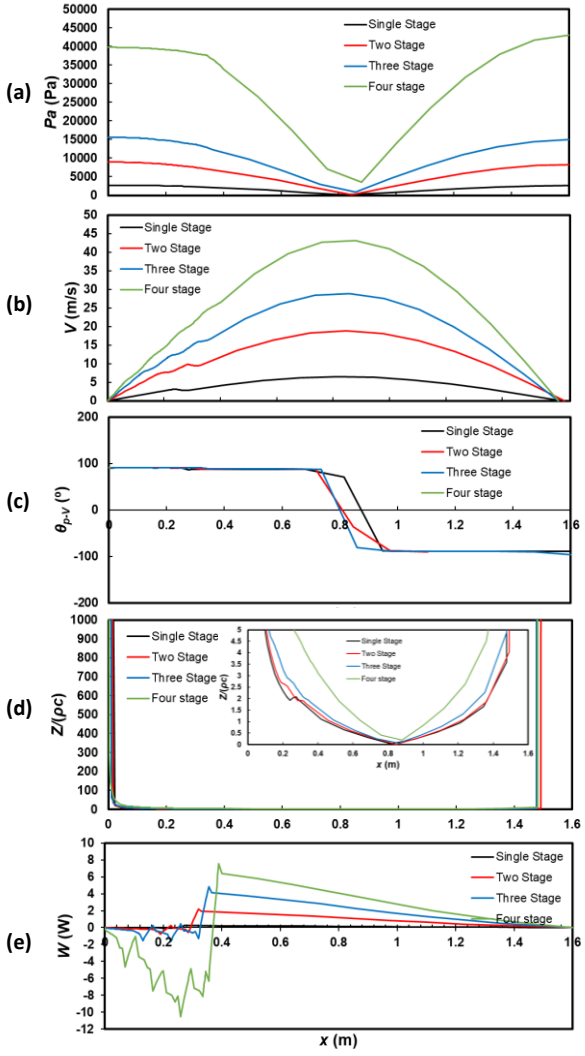

Fig. 8 Pressure amplitude P_a (a), velocity amplitude V (b), the phase difference between pressure and velocity Θ_{P-V} (c), specific acoustic impedance $Z/\rho c$ (d), and acoustic power W (e) distribution along the x-axis of the engine.

in production in the subsequent stages. In contrast to those of a traveling-wave engine, the unit stages can generate relatively uniform acoustic power in each stage when they are arranged with a distance of a quarter wavelength along the resonator (De Blok, 2010). We attributed this phenomenon to the asymmetrical arrangement of unit stages along the resonator, leading to nonuniform acoustic fields (Murti, Shoji and Biwa, 2023). However, we were not able to obtain convergent solution in the DeltaEC simulation when the unit stages were arranged symmetrically along the standing-wave thermoacoustic engine's resonator.

We also observed that increasing the number of unit stages significantly influences both total acoustic power production and thermal efficiency. Table 1 summarizes the total acoustic power production in the stack and the corresponding thermal efficiency for different unit stages. The total acoustic power production increased notably with the number of unit stages, achieving 3.8 W for two-unit stages, 10.03 W for three-unit stages, and 22.35 W for four-unit stages, respectively. A similar trend was observed for thermal efficiency. Thus, augmenting the number of unit stages in standing-wave thermoacoustic engines results in a lower onset temperature and improved acoustic power and thermal efficiency.

4. Conclusion

This study examines the influence of the number of unit stages on the performance of the standing wave thermoacoustic engine. We conducted stability analysis to determine the onset temperature ratio and DeltaEC calculation to elucidate the acoustic field distribution, respectively. Results showed that the onset temperature ratio decreases with the number of unit stages. However, with further increase in the number of unit stages, the onset temperature ratio tends to increase. The result showed that multiple unit stages need to be placed in the appropriate location to attain a low onset temperature. The lowest onset temperature of approximately 92°C is achieved when three- or four-unit stages are installed. Furthermore, acoustic field analysis reveals that increasing the number of unit stages does not significantly affect the phase difference between pressure and velocity or the specific acoustic impedance. In addition, the asymmetrical arrangement of unit stages along the resonator causes a nonuniform generation of acoustic power in the stack. Based on the elevation of acoustic power generation relative to the heating power required, increasing the number of unit stages in standing-wave thermoacoustic engines results in enhanced acoustic power and thermal efficiency. We found that four stages generated an acoustic power of 22.35 W and a thermal efficiency of 2.57%, respectively.

Acknowledgments

Prastowo Murti would like to extend sincere gratitude to Universitas Gadjah Mada for the invaluable support provided throughout this research.

Author Contributions: P.M., J.Z, & W.D.A.: Conceptualization, methodology, formal analysis, writing—original draft, I.S., A. W & T. B.; writing—review and editing, supervision, resources, project administration. All authors have read and agreed to the published version of the manuscript.

Funding: This research was funded by the Doctoral Competency Improvement Program Universitas Gadjah Mada Number 7743/UN1.P.II/Dit-Lit/PT.01.03/2023.

Conflicts of Interest: The authors declare that there are no conflicts of interests/competing interests.

References

Backhaus, S. and Swift, G. (1999) A thermoacoustic Stirling heat engine', *Nature*, 399, 335–338. https://doi.org/10.1038/20624.

Backhaus, S. and Swift, G.W. (2000) A thermoacoustic-Stirling heat engine: Detailed study, *The Journal of the Acoustical Society of America*, 107(6), 3148–3166. https://doi.org/10.1121/1.429343.

Biwa, T. Ueda, Y. Nomura, H. and Mizutani, U. (2005) Measurement of the *Q* value of an acoustic resonator, *Physical Review E*, 72(2), 26601.: https://doi.org/10.1103/PhysRevE.72.026601.

Biwa, T. Tashiro, Y. Nomura, H. Ueda, Y. and Yazaki, T. (2008) Experimental verification of a two-sensor acoustic intensity measurement in lossy ducts, *The Journal of the Acoustical Society of America*, 124(3), 1584–1590. https://doi.org/10.1121/1.2953311.

Biwa, T., Hasegawa, D. and Yazaki, T. (2010) Low temperature differential thermoacoustic Stirling engine, *Applied Physics Letters*, 97(3), 34102. https://doi.org/10.1063/1.3464554.

de Blok, K. (2010) Novel 4-stage traveling wave thermoacoustic power generator, in *American Society of Mechanical Engineers, Fluids Engineering Division (Publication) FEDSM*. https://doi.org/10.1115/FEDSM-ICNMM2010-30527.

de Blok Kees (2012) Multi-stage travelling wave thermoacoustic in practice, in *Proceedings of the 19th International Congress on Sound and Vibration*. International Institute of Acoustics and Vibration (IIAV).

Chi, J. Xu, J. Zhang, L. Wu, Z. Hu, J. and Luo, E. (2021) Study of a gas-liquid-coupled heat-driven room-temperature thermoacoustic refrigerator with different working gases, *Energy Conversion and Management*, 246, 114657. https://doi.org/10.1016/j.enconman.2021.114657.

Clark, J.P., Ward, W.C. and Swift, G.W. (2007) Design environment for low-amplitude thermoacoustic energy conversion (DeltaEC), *The Journal of the Acoustical Society of America*, 122(5), 3014. https://doi.org/10.1121/1.2942768.

Hamood, A. Jaworski, A. Mao, X. and Simpson, K. (2018) Design and construction of a two-stage thermoacoustic electricity generator with push-pull linear alternator, *Energy*, 144, 61–72. https://doi.org/10.1016/j.energy.2017.11.148.

Hiroaki, H., Keita, M. and Tetsushi, B. (2017) Stability Analysis of Thermoacoustic Gas Oscillations through Temperature Ratio Dependence of the Complex Frequency, *Journal of the Physical Society of Japan*, 86(10), 104401. https://doi.org/10.7566/JPSJ.86.104401.

Hyodo, H., Tamura, S. and Biwa, T. (2017) A looped-tube traveling-wave engine with liquid pistons, *Journal of Applied Physics*, 122(11),114902. https://doi.org/10.1063/1.4986409.

Jaworski, A.J. and Mao, X. (2013) Development of thermoacoustic devices for power generation and refrigeration, *Proceedings of the Institution of Mechanical Engineers, Part A: Journal of Power and Energy*, 227(7), 762–782. https://doi.org/10.1177/0957650913493622.

Jin, T., Yang, R. and Wang, Y. (2017) Low temperature difference thermoacoustic prime mover with asymmetric multi-stage loop configuration, *Sci Rep*, 7(7665). https://doi.org/10.1038/s41598-017-08124-5.

Li, D. Zhang, L. Wu, Z. and Luo, E. (2013) Numerical simulation and experimental investigation of a gas-liquid, double-acting traveling-wave thermoacoustic heat engine, *International Journal of Energy Research*, 37(15), pp. 1963–1970. https://doi.org/10.1002/er.3060.

Li, D. Chen, Y. Luo, E. and Wu, Z. (2014) Study of a liquid-piston traveling-wave thermoacoustic heat engine with different working gases, *Energy*, 158–163. https://doi.org/10.1016/j.energy.2014.05.034.

Murti, P. Setiawan, I. Widyaparaga, A. Utomo, A.B.S. and Nohtomi, M (2016) Influence of parameter on the performance of a standing-wave thermoacoustic prime mover, in *AIP Conference Proceedings*. https://doi.org/10.1063/1.4958538.

Murti, P. Takizawa, A. Shoji, E. and Biwa, T. (2021) Design and construction of multi-cylinder type liquid piston Stirling engine, in *E3S Web of Conferences*. EDP Sciences, p. 8003. https://doi.org/10.1051/e3sconf/202131308003

Murti, P., Shoji, E. and Biwa, T. (2023) Analysis of multi-cylinder type liquid piston Stirling cooler, *Applied Thermal Engineering*, 219, 119403. https://doi.org/10.1016/j.applthermaleng.2022.119403.

Piccolo, A. (2018) Design issues and performance analysis of a two-stage standing wave thermoacoustic electricity generator', *Sustainable Energy Technologies and Assessments*, 26, 17–27. https://doi.org/10.1016/j.seta.2016.10.011.

Rahman, M. R., Rahman, M. M., & Akter, R. (2023). Exploring the link between green energy, CO2 emissions, exchange rate and economic growth: Perspective from emerging South Asian countries. *International Journal of Renewable Energy Development*, 12(5), 930-941. https://doi.org/10.14710/ijred.2023.53168

Ramadan, I.A. Bailliet, H. Poignand, G. and Gardner, D. (2021) Design, manufacturing and testing of a compact thermoacoustic refrigerator, *Applied Thermal Engineering*, 189, 116705. https://doi.org/10.1016/j.applthermaleng.2021.116705.

Rott, N. (1969) Damped and thermally driven acoustic oscillations in wide and narrow tubes, *Journal of Applied Mathematics and Physics (ZAMP)*, 20, 230–243. https://doi.org/10.1007/BF01595562.

Rott, N. (1975) Thermally driven acoustic oscillations, part III: Second-order heat flux, *Journal of Applied Mathematics and Physics (ZAMP)*, 26, 43–49. https://doi.org/10.1007/BF01596277.

Setiawan, I. Utomo, A.B.S. Murti, P. Achmadin, W.N. and Nohtomi, M. (2019) Traveling-wave thermoacoustic engine with pressurized air working gas, in *AIP Conference Proceedings*. https://doi.org/10.1063/1.5095327.

Swift, G.W. (1988) Thermoacoustic engines, *The Journal of the Acoustical Society of America*, 84(4), 1145–1180. https://doi.org/10.1121/1.396617.

Swift, G.W. (2017) *Thermoacoustics: A Unifying Perspective for Some Engines and Refrigerators*. 2nd edn. Springer International Publishing.

Tamura, S., Hyodo, H. and Biwa, T. (2018) Experimental and numerical analysis of a liquid-piston Stirling engine with multiple unit sections, *Japanese Journal of Applied Physics*, 58(1), 17001. https://doi.org/10.7567/1347-4065/aae930.

Tijani, M.E.H. and Spoelstra, S. (2008) Study of a coaxial thermoacoustic-Stirling cooler, *Cryogenics*, (1), 77–82. https://doi.org/10.1016/j.cryogenics.2008.01.001

Timmer, M.A.G., de Blok, K. and van der Meer, T.H. (2018) Review on the conversion of thermoacoustic power into electricity, *The Journal of the Acoustical Society of America*, 143(2), 841–857. https://doi.org/10.1121/1.5023395.

Tominaga, A. (1995) Thermodynamic aspects of thermoacoustic theory, *Cryogenics*, 35(7), 427–440. https://doi.org/10.1016/0011-2275(95)93576-L.

Ueda, Y. Biwa, T. Mizutani, U. and Yazaki, T. (2004) 'Experimental studies of a thermoacoustic Stirling prime mover and its application to a cooler', *The Journal of the Acoustical Society of America*, 115(3), 1134–1141. https://doi.org/10.1121/1.1649333.

Wang, K. Sanders, S.R. Dubey, S. Choo, F.H. and Duan, F. (2016) Stirling cycle engines for recovering low and moderate temperature heat: A review, *Renewable and Sustainable Energy Reviews*, 62, 89–108. https://doi.org/10.1016/j.rser.2016.04.031.

Wang, K. Dubey, S. Choo, F.H. and Duan, F. (2017) Thermoacoustic Stirling power generation from LNG cold energy and low-temperature waste heat, *Energy*, 127, 280–290. https://doi.org/10.1016/j.energy.2017.03.124.

Wu, Z. Yu, G.Y. Zhang, L. Dai, W. and Luo, E. (2014) Development of a 3kW double-acting thermoacoustic Stirling electric generator, *Applied Energy*, 136, 866–872. https://doi.org/10.1016/j.apenergy.2014.04.105.

Yazaki, T., Biwa, T. and Tominaga, A. (2002) A pistonless Stirling cooler, *Applied Physics Letters*, 80(1), 157–159. https://doi.org/10.1063/1.1431695.

Yu, Z., Jaworski, A.J. and Backhaus, S. (2012) Travelling-wave thermoacoustic electricity generator using an ultra-compliant alternator for utilization of low-grade thermal energy, *Applied Energy*, 99, 135–145. https://doi.org/10.1016/j.apenergy.2012.04.046.

Zhang, X. Chang, J. Cai, S. and Hu, J. (2016) A multi-stage travelling wave thermoacoustic engine driven refrigerator and operation features for utilizing low grade energy, *Energy Conversion and Management*, 114, 224–233. https://doi.org/10.1016/j.enconman.2016.02.035.